

# Heterogeneous photo-Fenton treatment in the degradation of indigo carmine (IC) by using ZeoSonFe as a catalyst through an experimental design

Tratamiento foto-Fenton heterogéneo en la degradación de indigo carmín (IC) utilizando ZeoSonFe como catalizador, a través de un diseño experimental

I. Cosme-Torres\*, F.J. Illescas-Martinez

Tecnológico Nacional de México/Instituto Tecnológico de Toluca, Av. Tecnológico S/N, Colonia Agrícola Bellavista, C.P. 52149, Metepec, Estado de México, México.

Sent date: February 4, 2025; Accepted: July 1, 2025

#### **Abstract**

One of the most important advanced oxidation processes in the treatment of dyes is the photo-Fenton process using heterogeneous catalysts, according to its unique advantages: it allows the complete mineralization of the contaminant and the separation of the catalyst. A clinoptilolite-heulandite zeolite with Fe was conditioned as a catalyst. SEM analysis showed that ZeoSonFe is composed of characteristic cubic and polyhedral shaped crystals. EDS analysis of the ZeoSonFe showed an increase in Fe content in comparison to ZeoSonSod, furthermore it can be mentioned that Na<sup>+</sup> and Ca<sup>2+</sup> are the cations involved in the cation exchange of Fe<sup>2+</sup>. The first order rate constant increased with decreasing IC concentration, the  $k_1$  value was given in the following order BAA > BAB > BBB where three factors were studied: the concentration of IC at a low level (B= 100 mg L<sup>-1</sup>) and high level (A= 300 mg L<sup>-1</sup>), the amount of ZeoSonFe (B= 250 mg; A=1000 mg) and the dose of H<sub>2</sub>O<sub>2</sub> (B= 3 mmol; A= 9 mmol). *Keywords*: Indigo carmine, photo-Fenton, catalyst, experimental design.

#### Resumen

Uno de los procesos de oxidación avanzada más importantes en el tratamiento de colorantes es el proceso foto-Fenton mediante el uso de catalizadores heterogéneos; de acuerdo a sus ventajas únicas permite la mineralización completa del contaminante y la separación del catalizador. Se acondiciono una zeolita clinoptilolita-heulandita como catalizador. El análisis SEM permitió observar que la ZeoSonFe está compuesta de cristales característicos de forma cúbica y poliédrica. El análisis EDS de la ZeoSonFe mostró un aumento en el contenido de Fe en comparación con la ZeoSonSod, además se puede mencionar que el Na $^+$  y el Ca $^{2+}$  son los cationes que intervienen en el intercambio catiónico de Fe $^{2+}$ . La constante de velocidad de primer orden aumentó al disminuir la concentración del IC, el valor de  $k_1$  se dio en el siguiente orden BAA > BAB > BBA, donde se estudiaron tres factores: la concentración de IC a un nivel bajo (B = 100 mg L $^{-1}$ ) y nivel alto (A = 300 mg L $^{-1}$ ), la cantidad de ZeoSonFe (B = 250 mg; A = 1000 mg) y la dosis de H $_2$ O $_2$  (B = 3 mmol; A = 9 mmol).

Palabras clave: Indigo carmín, foto-Fenton, catalizador, diseño experimental.

\*Corresponding author. E-mail: ismael.ct@toluca.tecnm.mx; https://doi.org/10.24275/rmiq/IA25520 ISSN:1665-2738, issn-e: 2395-8472

## 1 Introduction

The existence of several dyes that are emitted to wastewater from different industries, mainly textile has caused several environmental problems. In most cases, water is returned to the river, lake, or soil without prior treatment due to the difficulty of implementing pollutant removal technologies (Gonzales-Condori et al., 2023; Ahmed & Mohamed, 2017). Indigo carmine (IC) dye, also known as acid blue 74 is considered as highly toxic indigo dye whose main component is indigotine, its chemical structure presents two important groups: NaSO3, which attributes the water-soluble property, and the chromophore group (a conjugated system of a C = C bond replaced by two NH groups and two C = O groups), which gives its color (Genázio et al., 2017; Mendes et al., 2015). IC is released in wastewater from the dyeing of polyester and denim fibers, it is estimated that approximately 5 to 20 % of the 20,000 t/year of dye used in this industry is lost during the dyeing process, it is usually resistant to aerobic biodegradation and is not easily degraded by conventional treatments, it is also used as a redox indicator in analytical chemistry and microscopic staining (Hernández-Gordillo et al., 2016; Arenas et al., 2017; Hadi et al., 2016).

Advanced Oxidation Processes (AOPs), provide an alternative for sustainable water recuperation, are effective chemical, photochemical or electrochemical methods to decompose persistent organic compounds in water (Ganiyu et al., 2015; Khataee et al., 2016). These have been of great interest for many years through oxidation reactions with highly efficient generation of hydroxyl radicals (\*OH)(Gagol et al., 2018). One of the most important AOPs in the treatment of dyes in effluents is the heterogeneous photo-Fenton process; this classic method is one of the most economical and fastest methodologies within the AOP. Due to its unique advantages of achieving complete mineralization of the pollutant reacting up to (CO<sub>2</sub>) and H<sub>2</sub>O), as well as relatively easy separation of the heterogeneous catalyst. Solid catalysts must meet a number of requirements such as: high activity in terms of pollutant removal, a leaching margin of active cations, stability over a wide pH and temperature range, high radical generation (\*OH)(Vázquez-Romero et al., 2024; Boczkaj & Fernandes, 2017). Iron (Fe) has emerged as a particularly promising candidate for catalysis, owing to its abundance, low cost, and low toxicity, Fe has undergone a renaissance in catalysis, fueled by advances in heterogeneous catalysis, owing to its several advantages. Heterogeneous Fe-based catalysts offer several advantages availability, costeffectiveness, and environmental friendliness, they can be easily separated from reaction mixtures, facilitating catalyst recovery and reuse. These catalysts

typically exhibit high stability and durability under reaction conditions. They exhibit high thermal and chemical stability, making them suitable for a wide range of reaction conditions. These catalysts often simplify purification processes by reducing product contamination with catalyst residues. Additionally, heterogeneous Fe catalysts can be engineered for high selectivity in specific reactions (Zhu *et al.*, 2023; Baruah *et al.*, 2024).

Zeolites are microporous crystalline solids formed by tetrahedral structures of aluminate  $(AlO_4)^{4-}$  and silicate (SiO<sub>4</sub>)<sup>5-</sup> connected at their vertices by oxygen atoms, with elements from groups I and II as exchange ions and various Si/Al ratios that describe the hydrophobicity of their surface. Due to their crystalline structure, porosity, shape, cavity size and hardness, zeolites present unique characteristics for their application in water treatment, including a high specific surface area associated with their porous structure, biocompatibility, ion exchange capacity, natural abundance and diverse adaptable porous structures (Leal-Perez et al., 2024; Ruiz-Baltazar, 2024; Samara et al., 2025). The Fenton-based processes involving zeolites also lead to the generation of hydroxyl radicals through the interaction of hydrogen peroxide with diverse iron species incorporated into the zeolites. For instance, iron-exchanged zeolites have been used for organic pollutant degradation through the reaction between the ferric ions in the zeolite and H<sub>2</sub>O<sub>2</sub> in the presence of UV light (Serna-Galvis et al., 2024). Several parameters influence the photo-Fenton process, in particular the pH of solution, the concentration of ferrous ions, the concentration of hydrogen peroxide, the stirring speed, the initial concentration of the dye, the volume of the solution, temperature, and contact time. For this reason, the factorial design is used to achieve the best overall optimization of a process by determining the effect of each factor on the response, as well as how the effect of each factor varies with the change in the level of the other factors. The interaction effects of different factors could be achieved using only the design of experiments (Elhalil et al., 2016; Barka et al., 2014). Therefore, the objective of this investigation was to establish a heterogeneous photo-Fenton treatment using a 23 factorial design. The effects analyzed were the amount of iron-conditioned zeolite, IC concentration, and the amount of H<sub>2</sub>O<sub>2</sub>. This heterogeneous photo- Fenton treatment is an alternative for sustainable water recovery.

## 2 Materials and methods

## 2.1 Conditioning of zeolite with Fe

Was used a natural zeolite of the clinoptiloliteheulandite type from Guaymas, Sonora, Mexico. The

zeolite was milled and sieved at 60 mesh (0.0098 in). For conditioning of the natural zeolite with NaCl, 100 g were placed in 650 mL of a 0.3 mol L<sup>-1</sup> NaCl solution (1:6.5), the mixture was kept in a refluxing system for 12 h. Then, the solution was decanted for a second reflux using a new NaCl solution. At the end of the sodium conditioning, the phases were separated and the solids were washed with deionized water before drying at 40 °C for 72 h, this zeolite is named ZeoSonSod. Then it was in contact the ZeoSonSod catalyst with a 0.2 mol  $L^{-1}$  FeSO<sub>4</sub>·7H<sub>2</sub>O solution (1:5 relation), the mix was stirred for 6 h at 60 °C. After the solids were washed with deionized water and finally, they were dried at 60 °C for 12 h. The obtained material (ZeoSonFe) was used as heterogeneous catalysts for IC removal tests.

#### 2.2 Characterization

The ZeoSonFe catalyst was characterized by infrared spectroscopy (FTIR), using a spectrophotometer; Varian model 640, equipped with accessory of attenuated total reflection (ATR), in the wavenumber range from 4000 to 400 cm<sup>-1</sup>. Specific surface area was analyzed by adsorption-desorption processes using nitrogen at a pressure of 72.18 KPa and a temperature of -196.15 °C using BELSORP-MAX equipment. The morphology was analyzed by using a scanning electron microscope; model JEOL JSM7800FEG at 10 Kv, the elemental chemical composition was determined by energy dispersion spectroscopy (EDS) with an Oxford Pentafet cooled, solid - state device.

#### 2.3 Photo-Fenton treatment

The photo-Fenton treatment was performed using a factorial design  $2^3$ , where three factors were studied: the concentration of dye [IC] (100 and 300 mg  $L^{-1}$ ); the dose of hydrogen peroxide  $H_2O_2$  (3 and 9 mmol); and the ZeoSonFe dosage (250 and 1000 mg), as shown in Tables 1 and 2.

Each experiment was performed in triplicate to reduce experimental error. In the experiments, a 500 ml reactor adapted with an ultraviolet light lamp (250 nm) was used. Subsequently, the IC solution was adjusted to optimum pH, using (HCl 0.1 mol  $L^{-1}$ ) and maintaining continuous stirring at 300 rpm experiments were carried out according to the combinations of the experimental design. Then samples of the treated solution were taken at different times (0 - 120 min), to evaluate the removal of the IC the samples were filtered using a syringe-type filter (0.45  $\mu m$ ) for the

separation of the ZeoSonFe catalyst. After filtration, the residual concentration was determined with an UV-Vis spectrophotometer (Thermo Spectronic Genesy 10 UV) at 612 nm of wavelength. The IC removal efficiency was calculated as follows Eq. (1). Where  $C_o$  is the initial IC concentration and  $C_t$  is the concentration of IC at time t in solution (mg  $L^{-1}$ ).

$$\% \text{Removal} = \left(\frac{C_o - C_t}{C_o}\right) \times 100 \tag{1}$$

### 2.4 Effect of pH and ORP

pH has been identified as a parameter that influences the photo-Fenton treatment, to determine the pH that presents the best IC degradation in aqueous solution, an IC solution (100 mg  $L^{-1}$ ) was used, this was adjusted to pH 3, 4 and 5 using (HCl 0.1 mol  $L^{-1}$ ). The pH was measured with a pH-meter (Denver Instrument 250), and then it was subjected to the photo-Fenton treatment heterogeneous using UV radiation (254 nm), 3 mmol H<sub>2</sub>O<sub>2</sub> and 250 mg of ZeoSonFe as a catalyst. The residual concentration of IC was determined using a UV-Vis spectrophotometer (Thermo Spectronic Genesy 10 UV) at a wavelength of 612 nm. The oxidation reduction potential (ORP) was monitored in the photo-Fenton treatment at pH 3, 4 and 5, the ORP measurement was performed during the degradation of the IC using an INTELLICAL ORP-REDOX MTC101 sensor.

# 3 Results and discussion

#### 3.1 FTIR analysis of ZeoSonFe

The FTIR spectrum of the catalyst (ZeoSonFe) is shown in (Figure 1), the vibrational characteristics of the catalyst during Na and Fe conditioning were analyzed. At a wavenumber of 3438 cm<sup>-1</sup> a broad band related to the hydroxyl groups (OH) of the (Si-OH) bond is observed, deformation of adsorbed water molecules is shown at 1632 cm<sup>-1</sup> (Pérez-González *et al.*, 2024; Paukshtis *et al.*, 2019), while at 1060 cm<sup>-1</sup> they are attributed to internal asymmetric vibrations of the tetrahedra and are susceptible to Si and Al content, the 787 cm<sup>-1</sup> weak intensity band corresponds to symmetrical stretching vibrations in the external structure of the tetrahedral bonds, at 605 cm<sup>-1</sup> the asymmetric stretching vibration

Table 1. Factors and levels for three independent variables

	1	
Factor	Max. Level (+)	Min. Level (-)
[IC] concentration (mg L <sup>-1</sup> )	300	100
ZeoSonFe catalyst dose (mg)	1000	250
[H <sub>2</sub> O <sub>2</sub> ] concentration %(mmol)	9	3

		2			
T-11 2 E		1	C	1	4 4 4
Iable / Exi	nerimentation	nian /	TOT	nnoto-Penton	treatment
Table 2. LA	perimentation	pran 2	101	photo i chion	ti catilicit

Experiment	IC concentration (mg L <sup>-1</sup> )	ZeoSonFe dose (mg)	H <sub>2</sub> O <sub>2</sub> concentration (mmol)
1	100	250	3
2	300	250	3
3	100	1000	3
4	300	1000	3
5	100	250	9
6	300	250	9
7	100	1000	9
8	300	1000	9

of the O-Si-O bonds of (SiO<sub>4</sub>) is observed, finally the band at 455 cm<sup>-1</sup> is attributed to internal bending vibrations of the Al-O-Si bond and corresponds to the Si/Al composition of each zeolite, while at 2360 cm<sup>-1</sup> it is assigned to the symmetric and asymmetric C=O modes that are associated with atmospheric CO<sub>2</sub>. It can be observed that the iron-conditioned zeolite does not show a significant change with the sodium-conditioned zeolite (ZeoSonSod) since the transition metal ion exchange does not produce alteration in the zeolitic netting (Abhijith *et al.*, 2020; Pérez-González *et al.*, 2024).

## 3.2 Scanning electron microscopy (SEM)

Elemental chemical composition (EDS) of the ZeoSonSod and ZeoSonFe catalyst, is shown in (Table 3). This is mainly composed of silicon (Si) and aluminum (Al), which proves the presence of aluminosilicates; aluminum oxide (Al<sub>2</sub>O<sub>3</sub>) and silicon oxide (SiO<sub>2</sub>) being the main component of the zeolite tetrahedron structure as reported by (Islam & Mohr, 2023; Yordanova et al., 2024; Biblioteca et al., 2023), and to a lesser percentage potassium (K), sodium (Na), calcium (Ca) and iron (Fe). EDS analysis of the ZeoSonFe catalyst indicated an increase in Fe, this occurs through the cation exchange of Na<sup>+</sup> and Ca<sup>2+</sup> it can also be observed that their weight percentages decrease due to equivalent substitution. In this work, the Si/Al ratio was 5.35 a value  $\geq$  5 is typical of zeolites rich in clinoptilolite, the importance of knowing the

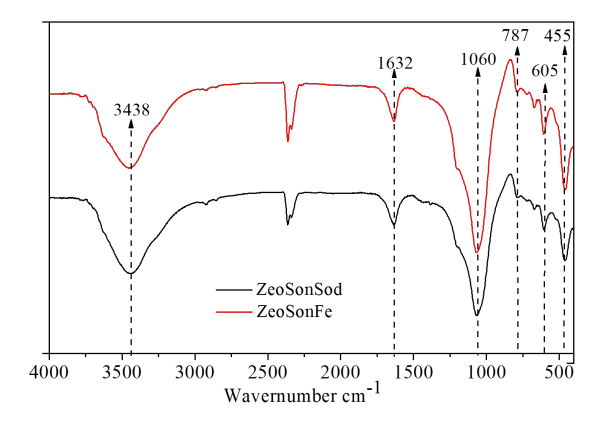


Figure 1. FTIR spectra of the ZeoSonSod and ZeoSonFe.

Si/Al ratio has been stated in terms of the coordination environment of aluminum species because it plays a relevant role in controlling the physical and chemical properties utilized for catalysts, adsorbates and ion-exchange materials, the Si/Al ratio is agreement with previous reports by (Barragán *et al.*, 2016). The (Figure 2) shows the micrograph at 20,000× magnifications of the 2a) ZeoSonSod and 2b) ZeoSonFe catalyst, both materials show an irregular morphology and surface, with characteristic crystals of polyhedral and cubic shaped. Finally, the ZeoSonFe catalyst presents a porous structure and agglomerates on the surface (Bhardwaj *et al.*, 2012; Barragán *et al.*, 2016).

#### 3.3 Surface area BET

It was found that the adsorption isotherms of the ZeoSonSod and ZeoSonFe catalyst belong to type IV, according to the International Union of Pure and Applied Chemistry (IUPAC) allows classifying these materials as mesoporous (between 2 and 50 nm) (Biblioteca et al., 2023). The average pore diameter value of the ZeoSonFe catalyst was 15.295 nm (Table 4), this diameter decreased with respect to the ZeoSonSod material due to the diffusion of metal ions that occurs through the macro, meso and microchannels in the zeolite structure, this characteristic is typical in mesoporous materials, with respect to surface area this was  $4.970 \text{ m}^2 \text{ g}^{-1}$  and a pore volume of  $1.141 \text{ cm}^3 \text{ g}^{-1}$ , the area was favored due to the cation exchange that occurred between the exchangeable cations of sodium zeolite and Fe<sup>2+</sup>, according to the crystal structure of clinoptilolite, the  $[SiO_4]^{4-}$  and  $[AlO_4]^{5-}$  tetrahedra are bonded in 0.9 nm wide layers; these layers are linked to each other by oxygen atoms in planar symmetry and form a three-dimensional structure. Sodium and calcium ions predominantly in channels A and B, and potassium preferentially located in channel C. This material is comparable to sodium zeolite since the conditioning process does not modify its anionic structure (Muhammad et al., 2024).

Table 3. Elemental chemical composition (EDS)

Table 3. Elemental c	nemicai compo	osition (EDS)
Composition (% w)	ZeoSonSod	ZeoSonFe
Si	$42.8 \pm 1.0$	$42.0 \pm 1.0$
O	$40.1 \pm 0.6$	$40.3 \pm 0.6$
Al	$8.0 \pm 0.9$	$7.8 \pm 0.9$
K	$4.3 \pm 0.9$	$4.4 \pm 0.9$
Na	$2.8 \pm 0.8$	$2.3 \pm 0.8$
Ca	$1.1 \pm 0.9$	$1.0 \pm 0.9$
Fe	$0.6 \pm 0.9$	$1.8 \pm 0.9$

Table 4.	Textural	parameters	of	zeolites

Material	Surface area	Total pore Volume	Average pore diameter
	$(m^2g^{-1})$	$(cm^3g^{-1})$	(nm)
ZeoSonSod	4.355	1.001	18.829
ZeoSonFe	4.970	1.141	15.295

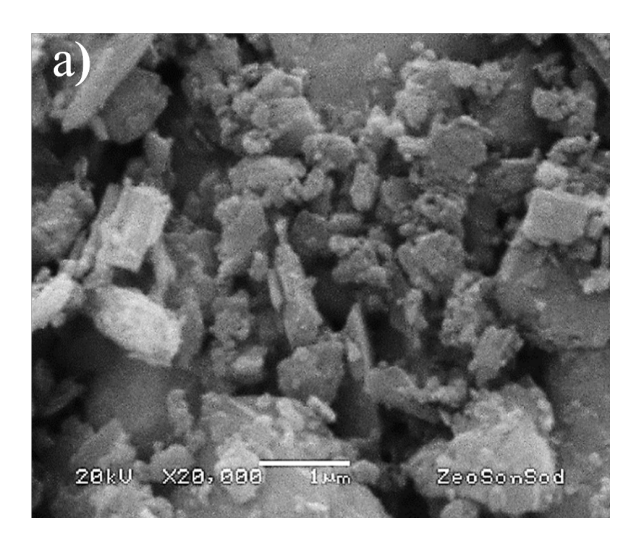


Figure 2a. Micrograph of the ZeoSonSod.

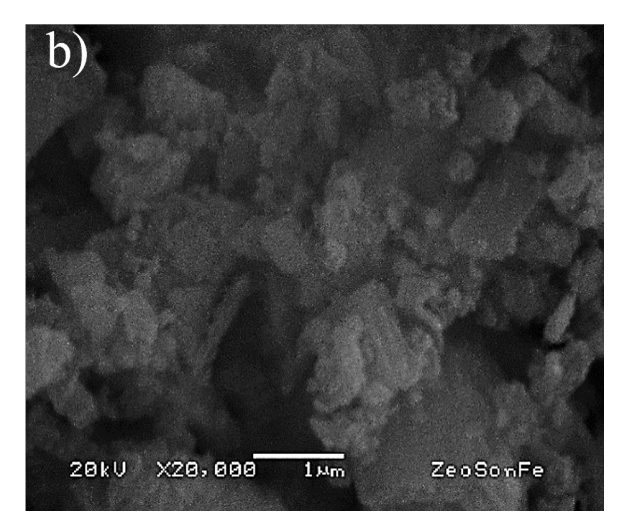


Figure 2b. Micrograph of the ZeoSonFe.

# 3.4 Oxidation reduction potential (ORP)

ORP values at pH 3 are shown in (Figure 3), there is a rapid increase from 398  $\pm$  5.2 mV to 520  $\pm$  4.3 mV in the first 20 min of treatment, the ORP was positive due to oxidation reactions generated by the (\*OH) radicals in solution until reaching a maximum value of  $542 \pm 4.6$  mV, however they decrease after 100 min of treatment due to the consumption of the (\*OH) radicals. The ORP at pH 4 and 5 showed low oxidation reactions reaching maximum values of  $508 \pm 3.3$  mV and  $460 \pm 3.5$  mV at 120 min of treatment. Azizia et al., (2020), mentions that ORP can be used as an important parameter to indicate the end of an oxidation reaction. Thus, the optimum pH value in this experimental design was 3, which showed better results since at a pH value  $\geq$  4 H<sub>2</sub>O<sub>2</sub> can decompose into H<sub>2</sub>O and O<sub>2</sub> molecules, as shown in Eq. (2) causing the yield of the reaction to decrease, while under very strong acidic conditions pH (2) it is possible that H<sub>2</sub>O<sub>2</sub> molecules can carry out a solvation process forming an oxonium ion [H<sub>3</sub>O<sub>2</sub>]<sup>+</sup>, these ions make H<sub>2</sub>O<sub>2</sub> more stable and reduce its reactivity with ferrous ions (Quadrado & Fajardo, 2017; Babuponnusami & Muthukumar, 2014).

$$2H_2O_2 \to 2H_2O + O_2 \tag{2}$$

# 3.5 Effect on pH

The optimum pH was 3 (Figure 4), at this value the greatest degradation of the dye occurred, obtaining  $6.00 \pm 0.20$  mg L<sup>-1</sup> of residual IC in 120 min of treatment, the acidic condition favors the degradation of the dye. At pH 5 and 4 the residual concentration of the dye was  $77.73 \pm 2.93$  mg L<sup>-1</sup> and  $34.27 \pm 1.88$  mg L<sup>-1</sup> respectively. The work carried out on the degradation of dyes treated by heterogeneous photo-Fenton has established an optimal pH value of 3, such as (Quadrado & Fajardo, 2017; Yaman & Gündüz, 2015; Basturk & Karatas, 2015), since a very low pH (pH < 3) is associated with the existence of complex iron [Fe(H<sub>2</sub>O)<sub>6</sub>]<sup>2+</sup> and [Fe(H<sub>2</sub>O)<sub>6</sub>]<sup>3+</sup> species that react more slowly with H<sub>2</sub>O<sub>2</sub> , as stated by (Javaid & Qazi, 2019).

An atomic absorption spectroscopy test was performed to analyze the amount of Fe leached from the ZeoSonFe catalyst in the treated solution after 120 min using a Perkin Elmer Model 31104 spectrophotometer. The results showed that at (pH 3), 0.245 mg L<sup>-1</sup> of leached Fe was obtained. As a reference, this value is lower than that established by the United States Environmental Protection Agency, since the maximum permitted limit is 0.3 mg L<sup>-1</sup> in drinking water. leaching of (Fe) cations from the catalyst is

reduced at low pH values, thereby improving catalyst performance ZeoSonFe.

#### 3.6 Experimental design

The degradation kinetics using a high concentration of IC (300 mg  $L^{-1}$ ) are shown in (Figure 5). The ABB combination corresponding to (300 mg  $L^{-1}$  of IC, 250 mg of ZeoSonFe and 3 mmol of  $H_2O_2$ ) obtained a residual concentration of 115.93  $\pm$  4.6 mg  $L^{-1}$  and a removal efficiency of 61.80  $\pm$  1.47 % in 120 min of treatment.

For the AAB (300 mg  $L^{-1}$  of IC, 1000 mg of ZeoSonFe and 3 mmol of H<sub>2</sub>O<sub>2</sub>) combination the residual concentration was  $55.74 \pm 5.21 \text{ mg L}^{-1}$ , the ABA (300 mg  $L^{-1}$  of IC, 250 mg of ZeoSonFe and 9 mmol of  $H_2O_2$ ) and AAA (300 mg  $L^{-1}$  of IC, 1000 mg of ZeoSonFe and 9 mmol of H<sub>2</sub>O<sub>2</sub>) combinations showed favorable results  $19.07 \pm 1.76 \text{ mg L}^{-1}$  and  $0.81 \pm 0.05$  mg L<sup>-1</sup> of residual IC, being the AAA combination the one that presented the best degradation treatment with a percentage of removal 99.73  $\pm$  0.01 %, the increase in the amount of catalyst generated a greater number of Fe<sup>2+</sup> catalytic sites which when coming into contact with H<sub>2</sub>O<sub>2</sub> molecules, generate a greater amount of (\*OH) radicals, these are responsible for the degradation of the IC. The low IC removal efficiencies are due to the increase in concentration, since it generates an increase in the internal optical density, this indicates that the higher the number of IC particles in the solution, the more impermeable it becomes to UV radiation. Therefore, H<sub>2</sub>O<sub>2</sub> will only be irradiated by a small amount of UV light, which generates less formation of (\*OH) radicals and less degradation of the IC (Castro-Peña & Durán-Herrera, 2014).

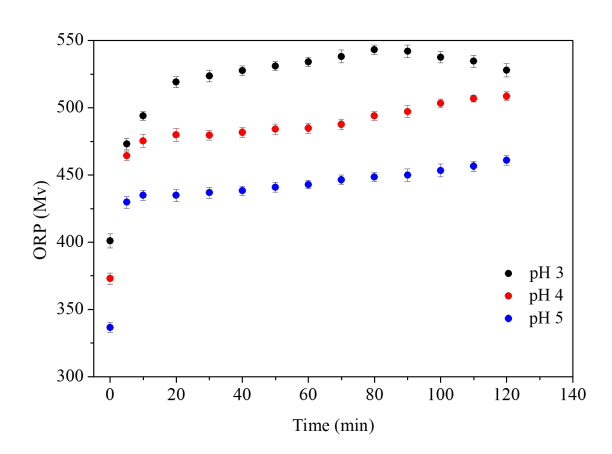


Figure 3. Effect of ORP on photo-Fenton treatment of IC. Conditions: [IC]=  $100 \text{ mg L}^{-1}$ , Cat.= 250 mg,  $H_2O_2= 3 \text{ mmol}$ , pH (3,4,5), Vol.= 500 mL

The results of the combinations in which a low concentration of IC (100 mg L<sup>-1</sup>) is used in the heterogeneous photo-Fenton treatment are shown in (Figure 6). The BAA combination corresponding to  $(100 \text{ mg L}^{-1} \text{ of IC}, 1000 \text{ mg of ZeoSonFe} \text{ and } 9 \text{ mmol})$ of H<sub>2</sub>O<sub>2</sub>) showed the best results in 20 min of treatment with a 97.09  $\pm$  0.10 % removal. The BAB (100 mg L<sup>-1</sup> of IC, 1000 mg of ZeoSonFe and 3 mmol of H<sub>2</sub>O<sub>2</sub>) combination also showed favorable results by using a greater amount of ZeoSonFe, which accelerated the formation of (OH) radicals, in 40 min a 98.62 ± 0.07 % removal efficiency was obtained, the BBB combination showed a removal efficiency of 94.06 ± 0.22 % in 120 min of treatment. The optimal amount of catalyst is important in photo-Fenton type treatments since an increase in the amount of catalyst generates a higher amount of solid particles in the solution that increasingly obstruct the photons emitted by the UV light due to the turbidity in the solution, consequently, the efficiency in the degradation of the dye decreases as reported by (Huy et al., 2020; Phan et al., 2018).

The degradation of the dye is initiated by the  $Fe^{2+}$  that has formed in the ZeoSonFe catalyst, this accelerates the catalytic decomposition of  $H_2O_2$  in solution, while it is oxidized by  $H_2O_2$  to  $Fe^{3+}$  (Fenton reaction). The  ${}^{\bullet}OH$  radicals that are generated attack the IC molecule adsorbed on the catalyst surface generating an increase in intermediates. Finally, the intermediates are converted to simpler molecules; as shown in the following reactions.

$$\equiv Fe^{2+} + H_2O_2 \rightarrow \equiv Fe^{3+} + \cdot OH + OH^-$$
 (3)

$$IC + \cdot OH \rightarrow Intermediates$$
 (4)

Intermediates 
$$\rightarrow CO_2 + H_2O$$
 (5)

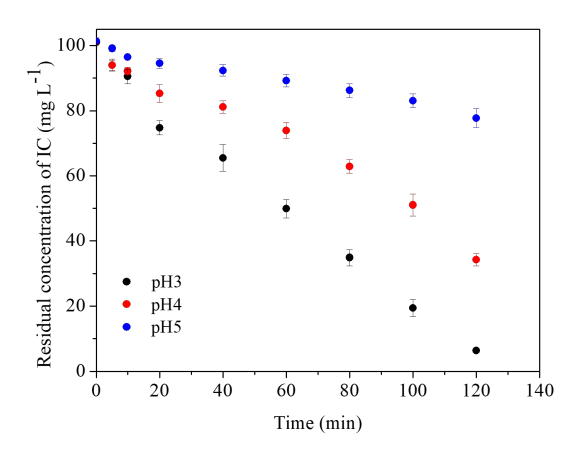


Figure 4. Effect of pH on the photo-Fenton treatment of IC. Conditions: [IC]=  $100 \text{ mg L}^{-1}$ , Cat.= 250 mg,  $\text{H}_2\text{O}_2$ = 3 mmol, pH (3,4,5), Vol.= 500 mL

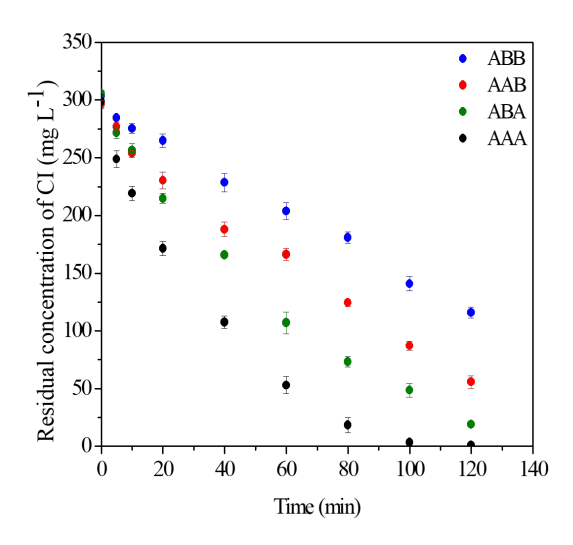


Figure 5. IC degradation kinetics (ABB, AAB, ABA, AAA)

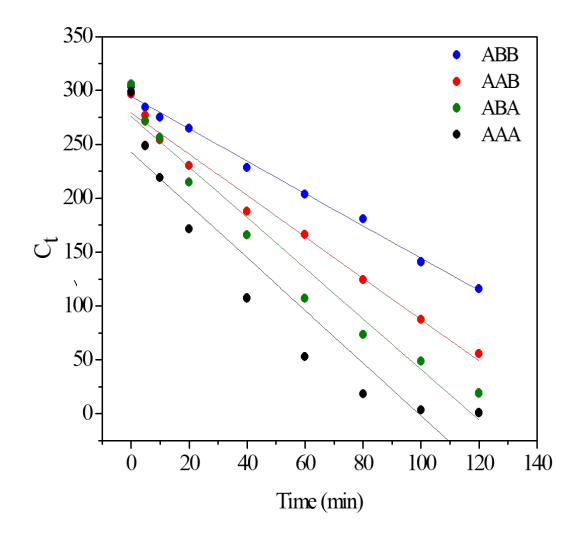


Figura 7. Linear fitting of zero-order kinetics (ABB, AAB, ABA, AAA)

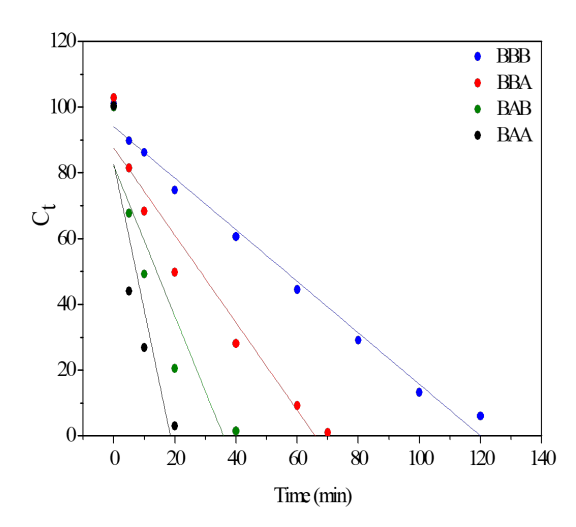


Figura 9. Linear fitting of zero-order kinetics (BBB, BBA, BAB, BAA)

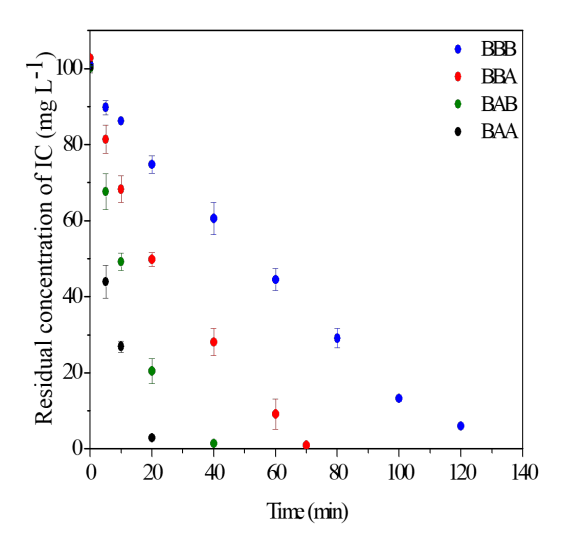


Figure 6. IC degradation kinetics (BBB, BBA, BAB, BAA)

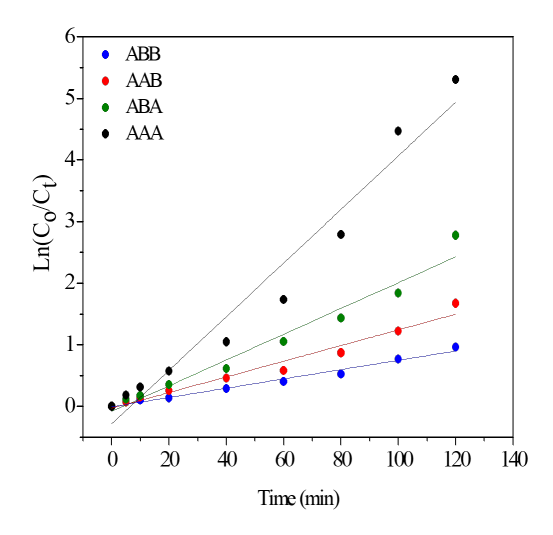


Figura 8. Linear fitting of First-order kinetics (ABB, AAB, ABA, AAA)

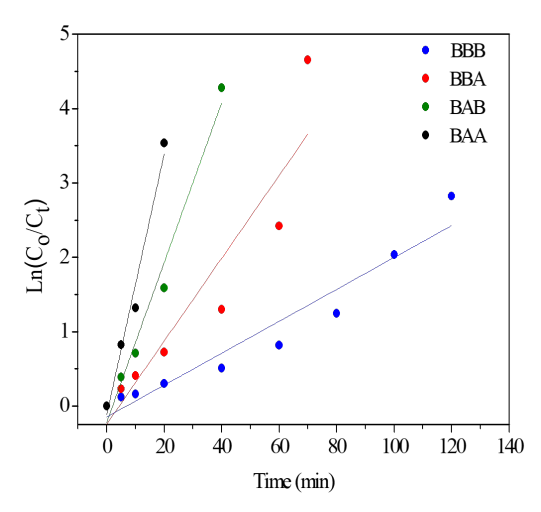


Figura 10. Linear fitting of First-order kinetics (BBB, BBA, BAB, BAA)

In the treatment of degradation, the concentration of  $H_2O_2$  is directly related to the generation of OH radicals, these can also be generated through the combination of UV light and  $H_2O_2$  by photolysis of  $H_2O_2$  where the UV radiation provides enough energy to break the O-O bond and generate the OH radicals, in photo-Fenton treatment the UV light significantly accelerates the degradation of the IC (Boczkaj & Fernandes, 2017). To describe the oxidative reaction in the degradation of IC, zero-order and first-order kinetics were used, Origin version 8.0 software was used for linear adjustments of the experimental data, the kinetic models are presented in the following equations:

Zero-order model:

$$C_t = C_0 - k_0 \cdot t \tag{6}$$

First order model:

$$\ln \frac{C_0}{C_t} = k_1 t \tag{7}$$

Where  $k_0$  and  $k_1$  are the rate constants of the kinetics reaction, t is the reaction time,  $C_0$  is the equilibrium concentration of the dye and the concentration of the dye after time t is  $C_t$ , to investigate the degradation of IC as a function of time, the degradation rate constant and the half-life of the reaction were calculated. The half-life  $t_{1/2}$ , indicates the time required for the concentration to decrease to 50% of its initial concentration. This value is determined according to equation (8), (Sirajudheen & Meenakshi, 2019; Asaduzzaman *et al.*, 2024).

half-life time:

$$t_{1/2} = \frac{0.693}{k_1} \tag{8}$$

Where:  $t_{1/2}$  = half-life time;  $k_1$ = Speed Constant (min<sup>-1</sup>).

Regarding the degradation kinetics, the experimental data were fitted to the zero-order and first-order kinetic model (Figure 7 and 8), it is observed that the value of the rate constant  $k_0$  is presented according to the following order AAA > ABA > AAB > ABB, this relationship corresponds with the degradation percentages of the IC.

The values of the velocity constant using a low concentration of dye were determined from Figures (9 and 10). The first order rate constant increased with decreasing IC concentration (100 mg  $L^{-1}$ ), the  $k_1$  value was given in the following order BAA > BAB > BBA > BBB these combinations achieved degradation percentages above 90 %, however, the degradation time was an important parameter since the BAA combination degraded the IC in 20 min with a  $t_{1/2}$  of 3.95 min and  $k_1$  of 0.1752 min<sup>-1</sup>.

### 3.7 *IC degradation*

To verify the maximum absorbance points of the IC in aqueous solution, a UV-vis absorption spectrum was performed in a range of 200 to 800 nm. The chromophore group is present in the 612 nm band, which gives the IC molecule its characteristic color (blue). The signal at 286 nm is related to the amino group, at 252 nm it is attributed to the carbonyl group, while the signal at 205 nm corresponds to the resonance of the aromatic ring (Ristea & Zarnescu, 2023). The degradation of IC is observed in the UV-vis spectrum (Figure 11). The absorption signals at 286 and 612 nm decrease, causing the break of the C=C double bond. This bond break is associated with the use of •OH radicals to produce isatin 5-sulfonic acid; after 20 minutes of treatment, a new band is observed at an  $\lambda$  of 410 nm. This is attributed to the formation of isatin, as reported by (Bernal et al., 2013). Subsequently, the IC molecule continues to be oxidized by OH radicals to form oxalic acid, which is mineralized into CO<sub>2</sub>.

Table 6 presents relevant literature from different studies using heterogeneous photo-Fenton treatment and/or advanced oxidation processes for IC degradation through synthetic solutions. The authors consider the amount of catalyst, dye concentration, H<sub>2</sub>O<sub>2</sub>, and pH; these parameters have been studied with effective and reproducible results. According to the reports in this work, ZeoSonFe as a heterogeneous catalyst achieves high IC degradation rates. The efficiency of the ZeoSonFe/UV/H<sub>2</sub>O<sub>2</sub> treatment is higher than that reported in terms of the initial IC concentration with other research works.

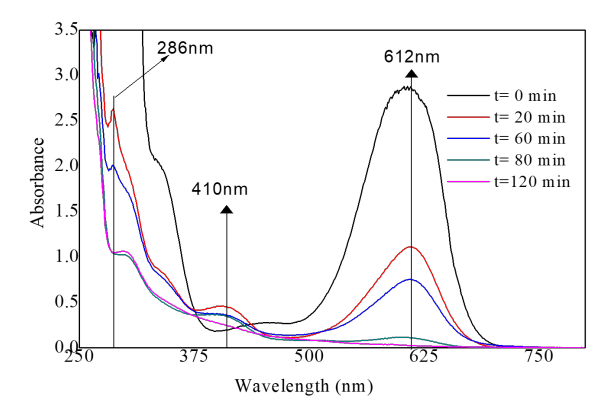


Figure 11. UV-vis spectrum in IC degradation measured at different times.

# 3.8 Statistical analysis of the experimental design

Statistical analysis in the heterogeneous photo-Fenton treatment was performed using the statistical software MINITAB 19. The analysis of variance provides the estimate of the effects of each factor, with a significance value  $\alpha = 0.05$ . To know the effect, it is sufficient to

Table 5. Kinetic parameters of the zero-order and

	first-order mo		
Kinetic model	Experiment	<sub>0</sub> (L <sup>-1</sup> min <sup>-1</sup> )	$R^2$
	ABB	1.501	0.993
Zero order	AAB	1.920	0.985
Zero order	ABA	2.348	0.959
	AAA	2.447	0.881
	Experiment	$_1(\min^{-1})$	$R^2$
	ABB	$7.54 \times 10^{-3}$	0.980
First order	AAB	$1.27 \times 10^{-2}$	0.966
	ABA	$2.09 \times 10^{-2}$	0.962
	AAA	$4.35 \times 10^{-2}$	0.956
Kinetic model	Experiment	$_0 (L^{-1} \min^{-1})$	$R^2$
	BBB	0.7835	0.9857
Zero order	BBA	1.3294	0.9337
Zero order	BAB	2.2865	0.8227
	BAA	4.4629	0.7682
	Experiment	$_1(\min^{-1})$	$R^2$
	BBB	$2.14 \times 10^{-2}$	0.9306
First order	BBA	$5.57 \times 10^{-2}$	0.8492
	BAB	0.1074	0.9738
	BAA	0.1752	0.9691

make it vary between low and high levels, the results presented in (Table 7) show P values lower than the significance level, which indicates a relationship between the factors and the degradation of the IC. Therefore, the concentration of IC, the amount of ZeoSonFe catalyst, the amount of H2O2 have an important effect. The ZeoSonFe catalyst with H2O2 has less statistical interaction, but it cannot be eliminated because the interaction with the three factors is important, an increase in the amount of catalyst results in a larger surface area improving the degradation of the IC. The coefficient of determination was also determined, which was 99.38 %, this being acceptable in the model, these indicators show how well the mathematical model adjusts to the residual value obtained in the degradation of the IC.

The following equation is based on a transformation of the data to obtain a normality, this equation suggests the control to the model and can indicate what is attributed to the response, which shifts the value of the residual in the heterogeneous photo-Fenton treatment.

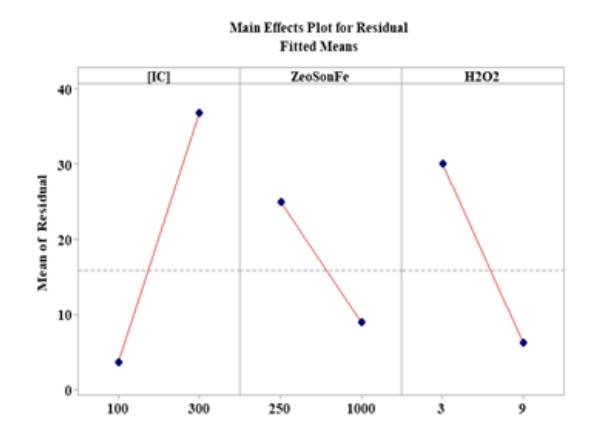
$$\begin{split} Residual^{0.266248} &= 1.197 + 0.010436 \ IC - 0.001691 \\ ZeoSonFe - 0.1323 \ H_2O_2 + 0.0000041 \ IC \cdot ZeoSonFe \\ - 0.000197 \ IC \cdot H_2O_2 + 0.000356 \ ZeoSonFe \cdot H_2O_2 - 0.0000021 \ IC \cdot ZeoSonFe \cdot H_2O_2 \end{split}$$

The effect of the system, represented graphically, is composed of the residual data obtained in the degradation of CI. Figure (12) shows the levels of each

factor (concentration of [IC] (100 and 300 mg  $L^{-1}$ ); dose of hydrogen peroxide (3 and 9 mmol); and the dose of ZeoSonFe (250 and 1000 mg)) at a low and high level, the wider the line, the greater the response of the variable to the degradation treatment. For example, the  $H_2O_2$  line is wider than the ZeoSonFe. In this case, the factor that refers to the amount of  $H_2O_2$  is important for the generation of  ${}^{\bullet}OH$  radicals. It also allows to visualize the residual concentration obtained according to the levels of each factor.

The Pareto diagram shown in (Figure 13), establishes the factors involved in the photo-Fenton treatment and the magnitude and importance of their presence can be determined; the graph represents the absolute value of each effect, Additionally, a reference line with a value of 2.31 is presented at the top of the plot (this value is statistically significant at the 0.05 level of significance using the current model terms), indicating that any bar extending beyond this can be considered potentially important in terms of IC degradation. The important factors such as the concentration of the IC, the amount of H<sub>2</sub>O<sub>2</sub>, followed by the amount of ZeoSonFe catalyst are factors that exceed the baseline which means that they could significantly affect the degradation process, and this can be confirmed with respect to the experimental data, by having a lower concentration of dye (100 mg  $L^{-1}$ ) the degradation time is much shorter than if a high concentration of dye (300 mg L<sup>-1</sup>) is used, this degradation time will depend on the amount of H<sub>2</sub>O<sub>2</sub> that is being used since it is an important reagent in the generation of OH radicals, by increasing this amount the degradation time decreases.

In Figure 14, specific regions are shown that mark the possible response that can be expected in the presence of a low concentration of IC 100 mg L<sup>-1</sup> a high amount of catalyst of 1000 mg of ZeoSonFe and 9 mmol of H<sub>2</sub>O<sub>2</sub>, using these high levels of the factors in the treatment can be seen the areas of operation, if we want to have areas where the residual concentration of the dye is less than  $10 \text{ mg L}^{-1}$  these parameters allows to have that concentration; both for concentration of 100 mg L<sup>-1</sup> and an initial concentration of 300 mg  $L^{-1}$  of dye see (Figure 15), this residual concentration is guaranteed when the peroxide level is 9 mmol. These residual contour figures can predict the values and levels where visually the residual concentration required in the treatment can be detected and make the availability of resources efficient. The areas in blue color guarantee the degradation of the IC and it is possible to predict the values to work with in order to have low residual values of residual dye, the more intense regions in green color can represent certain affectations in the treatment.



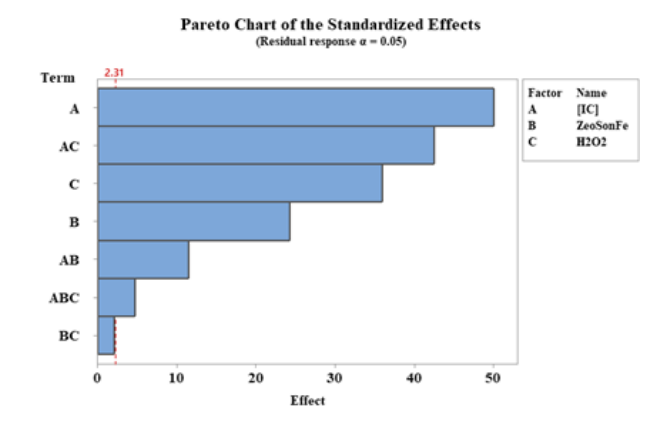


Figure 12. Main effects with ZeoSonFe as catalyst.

Figure 13. Pareto diagram of standardized effects.

Table 6. Comparison with previous work on the degradation of indigo carmine (IC)

Catalyst	Dye concentration	Decolorization % / Time	Reference
Fe-ZSM5	40 mg L <sup>-1</sup>	99 % of IC-10 min	Kasiri, <i>et al.</i> , 2008
HTCMgFe	100 mg L <sup>-1</sup>	100 % of IC-30 min	Cosme-Torres, et al., 2020
FeO/ZnO+SGC	69 mg L <sup>-1</sup>	95 % of IC-120 min	Reyes-Pérez, et al., 2023
FeO/ZnO+SGC	100 mg L <sup>-1</sup>	88 % of IC-120 min	Reyes-Pérez, et al., 2023
$MnFe_2O_4@BC$	$30 \text{ mg L}^{-1}$	50 % of IC-100 min	Ajibade & Nnadozie, 2020
ZnFe <sub>2</sub> O <sub>4</sub> @BC	$30 \text{ mg L}^{-1}$	65 % of IC-120 min	Ajibade & Nnadozie, 2020
ZnO-Bi <sub>2</sub> O <sub>3</sub> - xC <sub>3</sub> N <sub>4</sub>	50 mg L <sup>-1</sup>	45 % of IC-180 min	Huy, et al., 2020
ZeoSonFe	100 mg L <sup>-1</sup>	96 % of IC-120 min	This Work
	300 mg L <sup>-1</sup>	99 % of IC-120 min	This Work

Table 7. Coded coefficients for transformed response

Term	Effect	Coef	EE coef.	T-value	p-value	FIV
Constant		1.8274	0.0126	144.53	0.000	
IC	1.1452	0.5726	0.0126	45.29	0.000	1.00
ZeoSonFe	-0.5126	-0.2563	0.0126	-20.27	0.000	1.00
$H_2O_2$	-0.9262	-0.4631	0.0126	-36.63	0.000	1.00
IC*ZeoSonFe	-0.4234	-0.2117	0.0126	-16.75	0.000	1.00
$IC*H_2O_2$	-0.7341	-0.3670	0.0126	-29.03	0.000	1.00
ZeoSonFe*H <sub>2</sub> O <sub>2</sub>	0.0623	0.0311	0.0126	2.46	0.039	1.00
$IC*ZeoSonFe*H_2O_2$	-0.3696	-0.1848	0.0126	-14.62	0.000	1.00

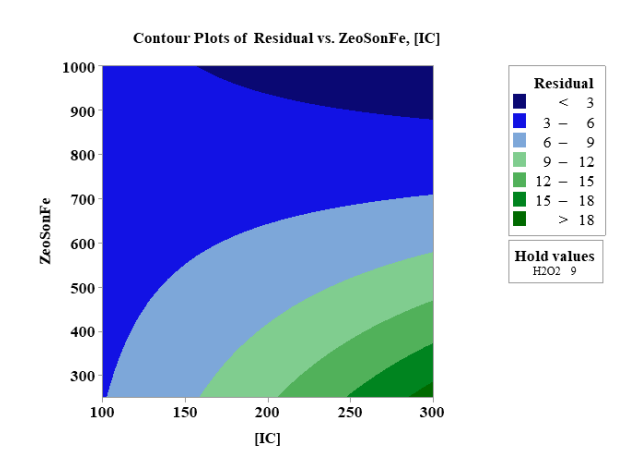


Figure 14. Residual contour Conditions: [IC]= 300 mg  $L^{-1}$ , Cat.= 1000 mg,  $H_2O_2 = 9$  mmol

## 4 Conclusions

The EDS analysis of the ZeoSonFe showed an increase in the Fe content compared to the ZeoSonSod, the Na<sup>+</sup> and Ca<sup>2+</sup> are the cations that intervene in the exchange of Fe<sup>2+</sup> because their percentage of them decreases (in % w). Oxidation Reduction Potential (ORP) at pH 3 showed a rapid increase in the first 20 min this is due to the generation of (\*OH) radicals that are carrying out oxidation of IC. The optimum pH was 3, at this value the greatest degradation of the dye occurred, obtaining  $6.00 \pm 0.20$  mg L<sup>-1</sup> of residual IC in 120 min of treatment, since a very low pH (pH < 3) is associated with the existence of complex iron  $[Fe(H_2O)_6]^{2+}$  and  $[Fe(H_2O)_6]^{3+}$  species that react more slowly with H<sub>2</sub>O<sub>2</sub>. The statistical analysis will allow to optimize the materials necessary for the degradation of the IC in different conditions of concentration, on the other hand the synthesized catalyst allowed to obtain good catalytic activity in the generation of hydroxyl radicals; this material will allow its use in later works of advanced oxidation in organic pollutants.

## Acknowledgements

To the Technological Institute of Toluca for the facilities and support for the development and dissemination of this research work, to the Mexican Council of Science and Technology (COMECyT) for its support in the program researchers for Mexico.

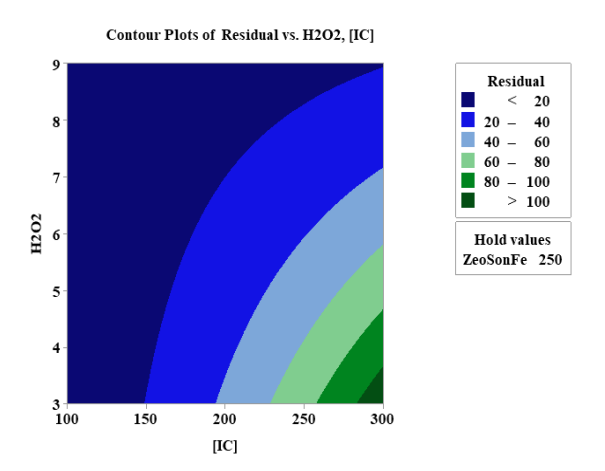


Figure 15. Residual contour Conditions: [IC]= 300 mg  $L^{-1}$ , Cat.= 250 mg,  $H_2O_2 = 9$  mmol

#### Nomenclature

SEM	Scanning Electron Microscopy
EDS	Energy Dispersion Spectroscopy
FTIR	Fourier Transform Infrared Spectroscopy
<b>IUPAC</b>	International Union of Pure and Applied Chemistry
IC	Indigo Carmine
<b>AOPs</b>	Advanced Oxidation Processes
ATR	Attenuated Total Reflection
(*OH)	Hydroxyl Radicals
ORP	Oxide Reduction Potential
EPA	Environmental Protection Agency
$t_{1/2}$	Half-life Reaction Time
$k_0, k_1$	Constants of the Kinetics Reaction

#### References

Abhijith, A.R., Srivastava, A.K., Srivastava. (2020). Synthesis and characterization of magnesium doped ZnO using chemical route. *Journal of Physics: Conference Series*, *1*, 1531. http://dx.doi.org/10.1088/1742-6596/1531/1/012005

Ahmed, M.A., & Mohamed, A.A. (2017). An efficient adsorption of indigo carmine dye from aqueous solution on mesoporous Mg/Fe layered double hydroxide nanoparticles prepared by controlled sol-gel route. *Chemosphere*, *174*, 280-288. http://dx.doi.org/10.1016/j.chemosphere.2017.01.147

Ajibade, P.A., & Nnadozie, E.C. (2020). Synthesis and structural studies of manganese ferrite and zinc ferrite nanocomposites and their use as photoadsorbents for indigo carmine and methylene blue dyes. ACS Omega, 5, 32386-32394. https://dx.doi.org/10.1021/

#### acsomega.0c04404

- Arenas, C.N., Vasco, A., Betancur, M., Martínez, J.D. (2017). Removal of indigo carmine (IC) from aqueous solution by adsorption through abrasive spherical materials made of rice husk ash (RHA). *Process Safety and Environmental Protection*, 106, 224-238. http://dx.doi.org/10.1016/j.psep.2017.01.013
- Asaduzzaman, Md, Hasan, N., Begum, K., Hoque, S.M.Z. (2024). Degradation kinetics of lycopene from red amaranth & preparation of winter melon jelly using this lycopene and comparison with commercial jelly. *Heliyon*, *10*, e31135. https://doi.org/10.1016/j.heliyon. 2024.e31135
- Azizia, E., Darsanja, A., Zakeric, H., Ghayebzadehd, M., Heidaripoure, Z. (2020). A study of the variations of oxidation-reduction potential, pH, and dissolved oxygen during photo-Fenton oxidation of methyl tert-butyl ether in the presence of a nanosized zero-valent iron particle, hydrogen peroxide, and ultraviolet radiation. Desalination and Water Treatment, 196, 238-246. https://doi.org/10.5004/dwt.2020.26044
- Babuponnusami, A., & Muthukumar, K. (2014). A review on Fenton and improvements to the Fenton process for wastewater treatment. *Journal of Environmental Chemical Engineering*, 2, 557-572. https://doi.org/10.1016/j.jece.2013.10.011
- Barka, N., Abdennouri, M., Boussaoud, A., Galadi, A., Baâlala, M., Bensitel, M., Sahibed-Dine, A., Nohair, K., Sadiq, M. (2014). Full factorial experimental design applied to oxalic acid photocatalytic degradation in TiO<sub>2</sub> aqueous suspensión. *Arabian Journal of Chemistry*, 7, 752-757. https://doi.org/10.1016/j.arabjc.2010.12.015
- Barragán, P.P., Macedo M.M.G., Olguín, M.T. (2016). Cadmium sorption by sodium and thiourea-modified zeolite-rich tuffs. *Journal of Environmental*, *52*, 39-48. https://doi.org/10.1016/j.jes.2016.03.015
- Baruah, M.J., Dutta, R., Zaki, M.E.A., Bania, K.K. (2024). Heterogeneous iron-based catalysts for organic transformation reactions: A brief overview. *Molecules*, 29, 3177. https://doi.org/10.3390/molecules29133177
- Basturk, E., & Karatas, M. (2015). Advanced oxidation of Reactive Blue 181 solution: A comparison between Fenton and Sono-Fenton Process. *Ultrasonics Sonochemistry*, 21,

- 1881-1885. http://dx.doi.org/10.1016/j.ultsonch.2014.03.026
- Bernal, M., Romero, R., Roa, G., Barrera, C.D., Torres, T.B., Natividad, R. (2013). Ozonation of índigo carmine catalyzed wIth Fe-pillared clay. *International Journal of Photoenergy*, *1*, 1-7. https://dx.doi.org/10.1155/2013/918025
- Bhardwaj, D., Sharma, M., Sharma, P., Tomar, R. (2012). Synthesis and surfactant modification of clinoptilolite and montmorillonite for the removal of nitrate and preparation of slow release nitrogen fertilizer. *Journal of Hazardous Materials*, 227-228, 292-300. https://doi.org/10.1016/j.jhazmat.2012.05.058
- Biblioteca, I., Sambucci, M., Valente, M. (2023). Zeolite-Clinoptilolite conditioning for improved heavy metals ions removal: A preliminary assessment. *Ceramics International*, 49, 39649-39656. https://doi.org/10.1016/j.ceramint.2023.09.319
- Boczkaj, G., & Fernandes, A. (2017). Wastewater treatment by means of advanced oxidation processes at basic pH conditions: A review. *Chemical Engineering Journal*, 320, 608-633. http://dx.doi.org/10.1016/j.cej.2017.03.084
- Castro-Peña, L., & Durán-Herrera, J. (2014). Degradation and decoloration of contaminated water with textile dyes using advanced oxidation processes. *Tecnología en Marcha*, 27(2), 40-50.
- Cosme-Torres, I., Macedo-Miranda, M.G., Martínez-Gallegos, S.M., González-Juárez, J.C., Roa-Morales, G., Illescas-Martínez, F.J., Jiménez-Becerril J. (2020). Synthesis of HTCMgFe for the degradation of indigo carmine through heterogeneous photo-Fenton treatment. *MRS Advances*, 5, 3273-3282. https://doi.org/10.1557/adv.2020.421
- Elhalil, A., Tounsandi, H., Elmoubarki, R., Mahjoubi, F.Z., Farnane, M., Sadiq, M., Abdennouri, M., Qourzal, S., Barka, S. (2016). Factorial experimental design for the optimization of catalytic degradation of malachite green dye in aqueous solution by Fenton process. *Water Resources and Industry*, *15*, 41-48. https://doi.org/10.1016/j.wri.2016.07.002
- Gagol, M., Przyjazny, A., Boczkaj, G. (2018). Wastewater treatment by means of advanced oxidation processes based on cavitation A review. *Chemical Engineering Journal*, 338, 599-627. https://doi.org/10.1016/j.cej. 2018.01.049

- Ganiyu, S.O., Hullebusch, E.D., Cretin, M., Esposito, G., Oturan, M.A. (2015). Coupling of membrane filtration and advanced oxidation processes for removal of pharmaceutical residues: A critical review. *Separation and Purification Technology*, 156, 891-914. https://doi.org/10.1016/j.seppur.2015.09.059
- Genázio, P.C., Valoura, R.R., Pavesi, T., Mendes, E.S., Costa, J.M., Veríssimo, F.C. (2017). Lethal and sub-lethal evaluation of Indigo Carmine dye and by products after TiO<sub>2</sub> photocatalysis in the immune system of Eisenia andrei earthworms. *Ecotoxicology and Environmental Safety*, *143*, 275-282. http://dx.doi.org/10.1016/j.ecoenv.2017.05.043
- Gonzales-Condori, E.G., Avalos-López, G., Gonzales-Condori, J., Mujica-Guzmán, A., Terán-Hilares, R., Briceño, G., Quispe-Avilés, J.M., Parra-Ocampo, P.J., Villanueva-Salas, J.A. (2023). Avocado seed powder residues as a promising bio-adsorbent for color removal from textile wastewater. *Revista Mexicana de Ingeniería Química*, 22(3), IA2370. https://doi.org/10.24275/rmiq/IA2370
- Hadi, M.D., Karimi, B., Sadege, M.R. (2016). The effect of aeration on advanced coagulation, flotation and advanced oxidation processes for color removal from wastewater. *Journal of Molecular Liquids*, 223, 75-80. http://dx.doi.org/10.1016/j.molliq.2016.08.019
- Hernández-Gordillo, A., Rodríguez-González, V., Oros-Ruiz, S., Gómez, R. (2016). Photodegradation of Indigo Carmine dye by CdS nanostructures under blue-light irradiation emitted by LEDs. *Catalysis Today*, 266, 27-35. http://dx.doi.org/10.1016/j.cattod. 2015.09.001
- Huy, B.T., Paeng, D.S., Thao, C.T.B., Phuong, N.T.K., Yong-Ill, L. (2020). ZnO Bi<sub>2</sub>O<sub>3</sub>/graphitic carbon nitride photocatalytic system with H<sub>2</sub>O<sub>2</sub>-assisted enhanced degradation of Indigo carmine under visible light. *Arabian Journal of Chemistry*, *13*, 3490-3800. http://dx.doi.org/10.1016/j.arabjc.2019.01.003
- Islam, M.S., & Mohr, B.J. (2023). Hydration kinetics of clinoptilolite zeolite blended ternary cementitious materials with fly ash and metakaolin. *Materials Today*. https://doi.org/10.1016/j.matpr.2023.03.468
- Javaid. R., & Qazi, U.Y. (2019). Catalytic oxidation process for the degradation of synthetic dyes: An overview. *International Journal of Environmental Research and Public Health*,

- 16, 2066. http://dx.doi.org/10.3390/
  ijerph16112066
- Kasiri, M.B., Aleboyeh, H., Aleboyeh, A. (2008). Degradation of acid Blue 74 using Fe-ZSM5 zeolite as a heterogeneous photo-Fenton catalyst. *Applied Catalysis B: Environmental*, 84, 9-15. http://dx.doi.org/10.1016/j.apcatb.2008.02.024
- Khataee, A., Gholami, P., Vahid, B. (2016). Heterogeneous sono-Fenton-like process using nanostructured pyrite prepared by Ar glow discharge plasma for treatment of a textile dye. *Ultrasonics Sonochemistry*, 29, 213-225. http://dx.doi.org/10.1016/j.ultsonch. 2015.09.012
- Leal-Perez, J.E., Almaral-Sanchez, J.L., Hurtado-Macias, A., Cortez-Valadez, M., Bórquez-Mendívil, A., García-Grajeda, B.A., Mendivil-Escalante, J.M., Flores-Valenzuela, J. (2024). Structural and chemical analysis of Zn ion exchange in thermally modified zeolite A4. Revista Mexicana de Ingeniería Química, 23(3), Mat24264. https://doi.org/10.24275/rmiq/Mat24264
- Mendes, E., Sousa, A., Forsin, D., de Paiva, D., Pavesi, T., Jimenez, M., Maldonado, M., Vieira, L., Costa, J. (2015). Photo-decolorization and ecotoxicological effects of solar compound parabolic collector pilot plant and artificial light photocatalysis of indigo carmine dye. *Dyes and Pigments*, 113, 571-580. http://dx.doi.org/10.1016/j.dyepig.2014.09.029
- Muhammad, R., Al-Muqati, N.S., Schulz, Axel., Alessa, A., Al-Otabi, Raja., Osman, A.I., Al-Fatesh, A.S. (2024). Temperature-induced modifications in natural zeolite clinoptilolite: effects on acidity and catalytic acetalization. *ChemNanoMat*, 10, e202400041. https://doi.org/10.1002/cnma.202400041
- Paukshtis, E.A., Yaranova, M.A., Batueva, I.S., Bal'zhinimaev, B.S. (2019). A FTIR study of silanol nests over mesoporous silicate materials. *Microporous and Mesoporous Materials*, 288, 109582. https://doi.org/10.1016/j.micromeso.2019.109582
- Phan, T.T.N., Nikoloski, A.N., Bahri, P.A., Li, D. (2018). Heterogeneous photo-Fenton degradation of organics using highly efficient Cu-doped LaFeO<sub>3</sub> under visible light. *Journal of Industrial and Engineering Chemistry*, 61, 53-64. http://dx.doi.org/10.1016/j.jiec. 2017.11.046

- Pérez González N. K., Díaz Guzmán D., Vargas Ramírez M., Legorreta García F., Chávez Urbiola E.A., Trujillo Villanueva L.E., Ramírez Cardona, M. (2024). Interzeolite conversion of a clinoptilolite-rich natural zeolite into merlinoite. *Sociedad española de cerámica y vidrio*, 63, 279-293. https://doi.org/10.1016/j.bsecv.2024.04.001
- Quadrado, R.F.N., & Fajardo, A.R. (2017). Fast decolorization of azo methyl orange via heterogeneous Fenton and Fenton-like reactions using alginate-Fe<sup>2+</sup>/Fe<sup>3+</sup> films as catalysts. *Carbohydrate Polymers*, *177*, 443-450. http://dx.doi.org/10.1016/j.carbpol.2017.08.083
- Reyes-Pérez, J.A., Roa-Morales, G., De León-Condes, C.A., Balderas-Hernández, P. (2023). Nanocomposites from spent coffee grounds and iron/zinc oxide: green synthesis, characterization, and application in textile wastewater treatment. Water Science & Technology, 88(6), 1547-1563. https://doi.org/10.2166/wst.2023.285
- Ristea, M. -E., & Zarnescu, O. (2023). Indigo carmine: between necessity and concern. *ournal of Xenobiotics*, 13(3), 509-528. https://doi.org/10.3390/jox13030033
- Ruíz-Baltazar, A.J. (2024). Advancements in nanoparticle-modified zeolites for sustainable water treatment: An interdisciplinary review. *Science of The Total Environment*, 946, 174373. https://doi.org/10.1016/j.scitotenv. 2024.174373
- Samara, F., Hamid, A.A.A., Gopal, V., Dronjak, L., Feghaly, F., Kanan, S. (2025). Modified zeolites for the removal of emerging bioresistive pollutants in water resources. *Catalysts*, *15*(2),138. https://doi.org/10.3390/catal15020138
- Serna-Galvis, E.A., Arboleda-Echavarría, J., Echavarría-Isaza, A., Torres-Palma, R.A. (2024).

- Removal and elimination of pharmaceuticals in water using zeolites in diverse adsorption processes and catalytic advanced oxidation technologies a critical review. *Environmental Science and Pollution Research*, 31, 63427-63457. https://doi.org/10.1007/s11356-024-35204-7
- Sirajudheen, P., & Meenakshi, S. (2019). Facile synthesis of chitosan-La<sup>3+</sup>-graphite composite and its influence in photocatalytic degradation of methylene blue. *International Journal of Biological Macromolecules*, 133, 253-261. http://dx.doi.org/10.1016/j.ijbiomac. 2019.04.073
- Yaman, C., & Gündüz, G. (2015). A parametric study on the decolorization and mineralization of C.I. Reactive Red 141 in water by heterogeneous Fenton-like oxidation over FeZSM-5 zeolite. *Journal of Environmental Health Science & Engineering*, 13(7), 2-12. http://dx.doi.org/10.1186/s40201-015-0162-6
- Yordanova, I., Hristov, S., Kolev, H., Todorova, S., Naydenov, A. (2023). Cobalt manganese ion-exchanged clinoptilolite supported catalysts for n-hexane oxidation. *Catalysis Today*, 423, 114267. https://doi.org/10.1016/j.cattod.2023.114267
- Vázquez-Romero, M., Abril-González, M., Pinos-Vélez, V., García-Zumalacarregui, J., Maldonado-Carchi, D., Miranda-Morales, D. (2024). Fenton process by volcanic ash to eliminate aniline of aqueous solution from the dyeing of toquilla straw crafts. *Revista Mexicana de Ingeniería Química*, 23(2), Cat24238. https://doi.org/10.24275/rmiq/Cat24238
- Zhu, F., Lu, G.P., Wang, F., Ren, E., Yu, Y., Lin, Y. (2023). Iron catalyzed organic reactions in water: A "Nature-Like" Synthesis. *Current Opinion in Green and Sustainable Chemistry*, 40, 100754. https://doi.org/10.1016/j.cogsc.2023.100754